ACS APPLIED MATERIALS & INTERFACES

Research Article

www.acsami.org

Gold Nanostructures on Flexible Substrates as Electrochemical Dopamine Sensors

Ming-Sheng Hsu,[†] Yu-Liang Chen,[†] Chi-Young Lee,[‡] and Hsin-Tien Chiu[†,*]

[†]Department of Applied Chemistry, National Chiao Tung University, Hsinchu, Taiwan 30050, R.O.C.

[‡]Department of Materials Science and Engineering, National Tsing Hua University, Hsinchu, Taiwan 30043, R.O.C.

Supporting Information

ABSTRACT: In this study, we fabricated Au nanowires (NWs), nanoslices (NSs), and nanocorals (NCs) on flexible polyethylene terephthalate (PET) substrates via direct current electrochemical depositions. Without any surface modification, the Au nanostructures were used as the electrodes for dopamine (DA) sensing. Among them, the Au NW electrode performed exceptionally well. The determined linear range for DA detection was 0.2−600 μM (N = 3) and the sensitivity was 178 nA/μM cm^2, while the detection limit was 26 nM (S/N = 3). After 10 repeated measurements, 95% of the original anodic current values were maintained for the nanostructured electrodes. Sequential additions of citric acid (CA, 1 mM), uric acid (UA, saturated), and ascorbic acid (AA, 1 μM) did not interfere the amperometric response from the addition of DA (0.1 μM).

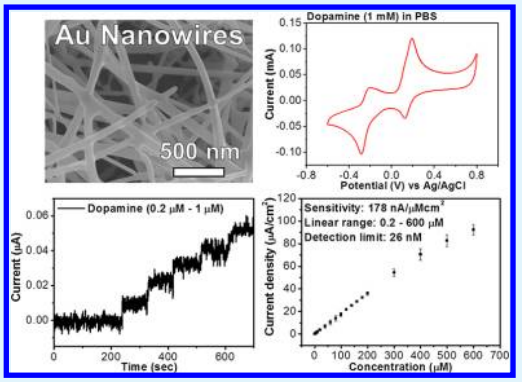

KEYWORDS: *gold, nanocoral, nanoslice, nanowire, electrodeposition, dopamine, sensor*

INTRODUCTION

Dopamine (DA) is an important neurotransmitter of catecholamine in human brain.[1] Several important diseases of the nervous system are associated with dysfunctions of the dopamine system, including Parkinson's disease,[2] Schizophrenia,[3] and attention deficit hyperactivity disorder (ADHD).[4] In addition, DA is available as an intravenous medication, which acts on the sympathetic nervous system, to produce effects such as increasing heart rates and blood pressure.[5] Thus, determination of DA in vivo/vitro becomes important in clinical medical practice. In recent years, several surface modification approaches have been intensively developed to increase the performance of electrochemical DA sensors.[6−22] These include noble metal nanoparticle (NP) decorations, polymer modifications, and enzyme modification. For example, noble metal (Pt, Pd, Cu, and Au) NPs are frequently deposited on the electrodes to improve the electrochemical responses from catalytic DA oxidations.[6−8,13,14] In another approach, the electrodes are modified with various polymer films. They can limit the access of interfering agents, such as ascorbic acid (AA) and uric acid (UA), at high concentrations in human body fluids to the electrode surfaces.[9,10,15−19] In addition, by using the enzyme recycling approach, the operating potential differences of the electrodes are lowered while the electrode sensitivities are improved.[11,20−22] Among these, electrodes fabricated from metal NPs express high surface areas with increased quantities of active sites for reactions. Thus, the electrode performance is effectively enhanced, as observed in many electrochemical devices.[33−36] For biosensing electrodes, Au is an excellent choice due to its conductivity, stability, and biocompatibility. Incorporating metal NPs onto flexible substrates provides opportunities for many bendable biosensing electrodes. Advantages of flexible electrodes include lightweight, thin in thickness, high portability, and resistance to mechanical impact tension, torsion, and bending. Thus, the developments are well-suited for biochip, medical product, and minimally invasive implantable device applications.[26−32] Previously, we have reported electrochemical growths of nanostructured Au on hard substrates, that is, Si wafer and glass.[33−35] Recently, we have developed a process to grow Au nanowires (NWs), nanoslices (NSs), and nanocorals (NCs) on flexible commercial transparencies made from polyethylene terephthalate (PET).[36] Here, we report our preliminary investigations on using the Au nanostructures as the electrodes, without surface modifications, for electrochemical sensing of DA. Since the nanostructured Au electrodes express high surface areas, we expect they exhibit excellent performance. Our discoveries are presented below.

RESULTS AND DISCUSSION

Growth and Characterization of Gold Nanostructures.

By using fabrication processes similar to the ones reported before, the Au nanostructures were grown on flexible PET substrates as described below.[34−36] A thin Ti layer and an Au film were deposited by e-gun evaporation on a PET transparency. The fabrication steps and the photographic

Received: July 25, 2012
Accepted: September 28, 2012
Published: September 28, 2012

views are shown in Figure S1 in the Supporting Information. Magnified scanning electron microscopic (SEM) images of the as-prepared Au/Ti/PET substrate are displayed in Figure S2 (Supporting Information). Figure 1A displays the SEM image

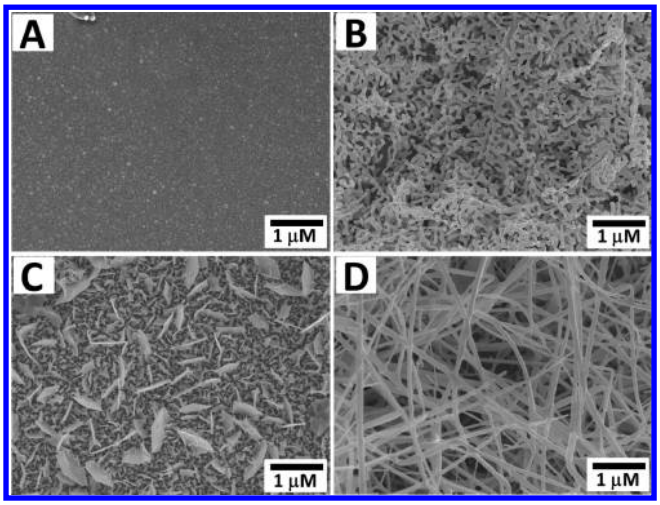

Figure 1. SEM images of Au nanostructures: (A) film, (B) NCs (1.6 V, 288 K), (C) NSs (1.0 V, 288 K), and (D) NWs (0.7 V, 298 K) grown on flexible PET substrates.

of the flat Au surface with nanosized grains, which served as the film electrode in this study. In addition, it was employed as the seeding layer for the electrochemical deposition of Au nanostructures by using the experimental setup shown in Figure S2 (Supporting Information).[37−39] By controlling the electrochemical deposition parameters, Au NCs, NSs, and NWs were grown. Their SEM images are shown in Figure 1B−D. Detailed SEM, transmission electron microscopic (TEM), and electron diffraction (ED) data are shown in Figures S4−S6 in the Supporting Information. From the images, the width of the NC branch, the thickness of the NS, and the diameter of the NW are determined to be 100−200 nm, 13−18 nm, and 80−120 nm, respectively. These Au nanostructures are similar to the ones grown directly on hard substrates reported before.[33−36] By integrating the reduction currents recorded during the electrodepositions, as shown in Figure S7 (Supporting Information), the deposited Au weights were calculated using Coulomb's law. Cyclic voltammograms (CV) of the nanostructured Au electrodes in H_2SO_4(aq) are displayed in Figure S8 (Supporting Information). From the data, real surface areas (RSAs) of the Au nanostructures were estimated.[40] The electrochemical active surface areas (EASA) are calculated from the CV data of $K_4Fe(CN)_6/K_3Fe(CN)_6$ (2.5 mM) shown in Figure S9 in the Supporting Information. A summary of the features of the nanostructured Au electrodes fabricated in this study are listed in Table 1. Clearly, the RSA of the film electrode with a flat surface, 0.13 cm^2, is much smaller than the values 2.74−3.15 cm^2 of the other nanostructured electrodes. The EASA data of the electrodes also demonstrate a similar result. Here, the NW electrode provides the highest EASA, 0.151 cm^2. The SEM images of other Au nanostructures grown at different applied voltages and temperatures (Table S1 in the Supporting Information) are presented in Figures S10 and S11 (Supporting Information). As shown in the figures, growths of the Au nanostructures are highly influenced by a combination of reaction parameters. These include the reaction temperature, the applied potential, and the concentrations of reactants and other reagents. They all affect the reactions in specific ways. At low temperatures and low potentials, the crystal growths are restricted by the presence of the surfactant molecules and NO_3^- ions. Under a favorable condition, the growth of a specific crystal facet could either be enhanced or restricted. As a result, crystals could grow anisotropically, for example, into nanoslices and nanowires. On the other hand, at high temperatures and high potentials, the growth rates are increased. Consequently, the crystals enlarge isotropically into less defined particles. The growth mechanisms have been reported and discussed in detail in our previous studies.[23−26]

Electrochemical Catalysis of Dopamine on Nanostructured Gold Electrodes. Representative cyclic voltammograms (CV) of DA (1 mM) in phosphate buffer solutions (PBS, 0.1 M, pH 7.40) on various Au electrodes are presented in Figure 2. The first and the second CV cycles are shown for

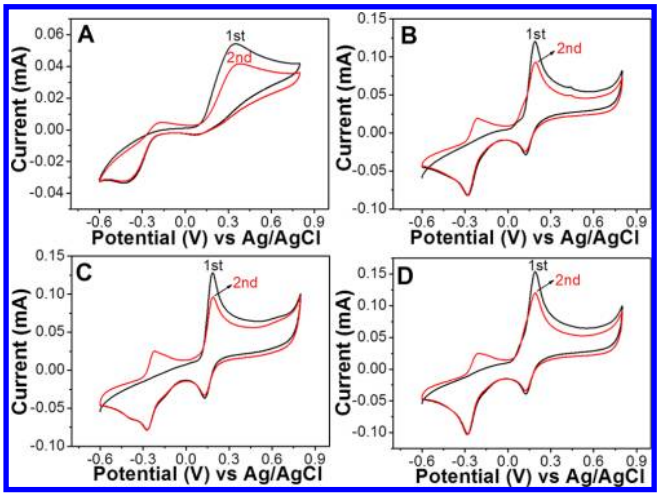

Figure 2. First (black) and second (red) cyclic voltammograms (scan rate 50 mV/s) of DA (1 mM) in PBS (0.1 M, pH 7.40) on nanostructured Au electrodes: (A) film, (B) NC, (C) NS, and (D) NW.

Table 1. Summary of Nanostructured Au Electrodes

sample	geometric area (cm^2)	grown condition[a] potential (V)	grown condition[a] temp. (K)	morphology	deposited weight (μg)	real surface area (cm^2)	electrochemical active surface area (cm^2)
film	0.25	N.A.[b]	N.A.[b]	grain size < 10 nm	N.A.[b]	0.13	0.101
NC	0.25	1.6	288	width: 100−200 nm	212	2.74	0.138
NS	0.25	1.0	288	thickness: 13−18 nm	20.0	2.92	0.138
NW	0.25	0.7	298	diameter: 80−120 nm length: several μm	59.4	3.15	0.151

[a]In $HAuCl_{4(aq)}$ (5 mM), $CTAC_{(aq)}$ (10 mM), and $NaNO_{3(aq)}$ (20 mM) for 24 h. [b]N.A.: not applicable.

dx.doi.org/10.1021/am301452b | ACS Appl. Mater. Interfaces 2012, 4, 5570−5575

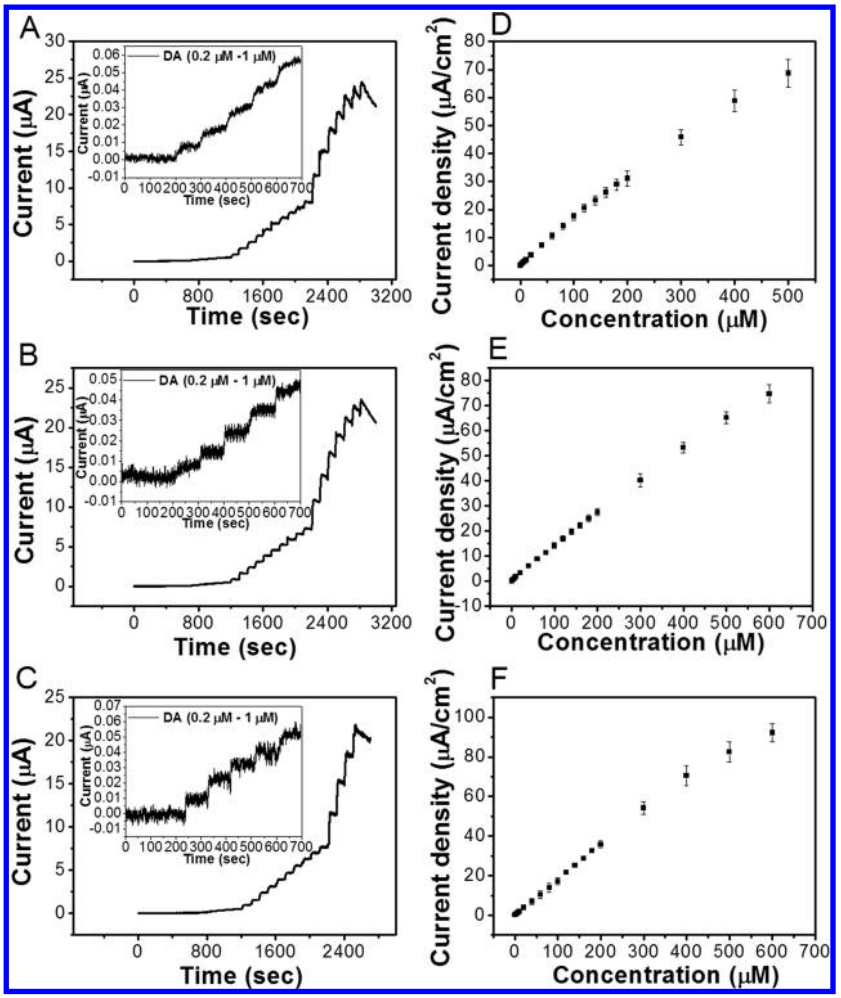

Figure 3. Amperometric responses (0.200 V) of successive addition of DA in PBS on Au electrodes: (A) NC, (B) NS, and (C) NW. Variations of current densities against DA concentrations using Au electrodes: (D) NC, (E) NS, and (F) NW.

each electrode. The most obvious observation found in Figure 2 is the lack of an initial anodic peak near −0.2 V for each one of the Au electrodes. This is because leucodopaminochrome (LDAC), a reaction product, is yet to be formed in the first cycle. More detailed explanations are discussed below by using the CV scans obtained from the Au NW electrode. As shown in Figure 2D, the second CV scan displays an anodic peak at 0.192 V and a cathodic peak at 0.124 V. They are assigned to the oxidation of DA to *o*-dopaminoquinone (DAQ) and the reduction of DAQ back to DA, respectively.[41] At pH 7.4, DAQ undergoes intramolecular cyclization to form LDAC.[42] Thus, a redox pair with a cathodic peak at −0.282 V and an anodic peak at −0.201 V in the second CV scan are assigned to the LDAC/dopaminochrome (DAC) redox couple. The CV scans of the other nanostructured Au electrodes, that is, NC and NS ones, show similar behaviors (Figure 2B,C). On the other hand, for the film electrode, the DA/DAQ redox couple displays an anodic peak at 0.352 V and a cathodic peak at 0.066 V in the CV scans shown in Figure 2A. Here, the cathodic peak current is much smaller than the anodic peak current. This indicates that the electrochemical reactions of these species on the Au film electrode are irreversible. Besides, on the film electrode, the redox peak difference ΔEp is 0.286 V. In contrast, as shown in Figure 2B−D, ΔEp values of the nanostructured Au electrodes are below 0.07 V. The peak currents increase largely as well. The observed data are summarized in Table S2 in the Supporting Information. They suggest that the nanostructured electrodes provided higher catalytic ability due to much better electron transfers than the film electrode did. The observations agree with literature reports well.[8,43−45] An example demonstrates that three-dimensional nanoporous Au provides higher surface area to induce faster electron transport than Au NPs electrode does.[46]

Amperometric Responses of Dopamine on Nanostructured Gold Electrodes. For a healthy human, the concentration of DA in circulation is about 10 nM while the value in synapse is 0.3−1 mM.[1] To determine the sensitivity and linear range of the nanostructured Au electrodes for DA detection, amperometric responses are displayed in Figure 3A−C. The data of the film electrode is not shown because of bad selectivity of Au film electrodes; this part is discussed later in the article. The response currents were monitored at a potential fixed at 0.200 V after successive additions of DA into a stirred PBS (0.1 M, pH 7.40) solution. In Figure 3D−F, each oxidative current density is plotted against the corresponding DA concentration to show a linear response for each electrode. The linear range of the NC electrode is 0.2−500 μM with a correlation coefficient r = 0.991 (N = 3). For the NS electrode, the linear range is 0.2−600 μM while the correlation coefficient r = 0.992 (N = 3). The NW electrode displayed a linear range 0.2−600 μM and a correlation coefficient r = 0.998 (N = 3). The detection limits are estimated to be 0.060 μM, 0.054 μM,

and 0.026 μM for NC, NS, and NW electrodes, respectively. The values are calculated from the following method: limit of detection (LOD) = σ/S, where σ = the standard deviation of the response and S = the standard deviation of y-intercept of the regression line.[47] From the amperometric data summarized in Table 2, the Au NW electrode presents the widest linear range, the highest sensitivity, and the lowest detection limit among all nanostructures. This is attributed to the largest RSA of the NW electrode.

Table 2. Summary of Parameters Derived from Amperometric Responses of DA on Nanostructured Au Electrodes

electrode	linear range (μM)	sensitivity (nA/(μM cm^2))	correlation coefficient (r)	detection limit (μM)[a]
NC	0.2−500	161	0.991	0.060
NS	0.2−600	138	0.992	0.054
NW	0.2−600	178	0.998	0.026

[a]All S/N ratios are close to 3:1.

Fouling and Stability of Nanostructured Gold Electrodes. Previous reports indicated that adsorption of reaction products on bare electrodes degraded DA oxidation performance.[48,49] To assess whether the nanostructured Au electrodes fabricated in this study may suffer the same fouling effect, each one of the electrodes was measured 10 times successively in a DA (500 μM) containing PBS (0.1 M, pH 7.40) solution. Their current responses are shown in Figure S12 in the Supporting Information. After 10 measurements, 39.7%, 94.14%, 96.66%, and 95.13% of the original anodic currents of the film, NC, NS, and NW electrodes are retained, respectively. The film electrode's performance degrades significantly probably due to its low electron transfer efficiency so that more intermediates polluted the surface. For the nanostructured electrodes, only about 95% of their original performance has been retained, and their morphology has stayed the same as well, as displayed in Figure S13 in the Supporting Information.

Interferences from Ascorbic and Uric Acids to Amperometric Detection of Dopamine on Nanostructured Gold Electrodes. Ascorbic acid (AA) and uric acid (UA) coexist in physiological fluids commonly. This may hamper the electrochemical detection of DA. To understand if the nanostructured Au electrodes could reduce the interference, the following investigations were carried out. The first scans of the CV diagrams of AA (1 mM), UA (0.3 mM), and DA (1 mM) in PBS (0.1 M) are overlapped and presented together in Figure 4 for the film, NC, NS, and NW electrodes. Several differences are clearly visible. When nanostructured Au electrodes are employed, the current responses from DA are clearly enhanced several times more than the one generated by using the film electrode. Although the responses from AA and UA increase too, their increments are not as high. Also, all the oxidation peaks from the nanostructured electrodes have shifted negatively when they are compared with the ones from the film electrode. It means that the electrocatalytic activities toward DA, AA, and UA have been improved on the nanostructured Au electrodes. Generally, electrocatalytic activity enhances as oxidation overpotential decreases. All of the related CV data are summarized in Table S2 in the Supporting Information. The improvements are attributed to high RSAs of the nanostructures. They provide high density of active sites to promote charge transfer between the electrode surface and the reactants in the solution.[46,50−52] Each one of the nanostructured Au electrodes reacts distinctively toward AA, DA, and UA. On the film electrode, both AA and DA show broad and overlapping oxidation peaks. Thus, AA would interfere more with DA than UA does in amperometric detections. On the other hand, on nanostructured Au electrodes, the peak separations become prominent. We expect this character would enhance the amperometric performance.

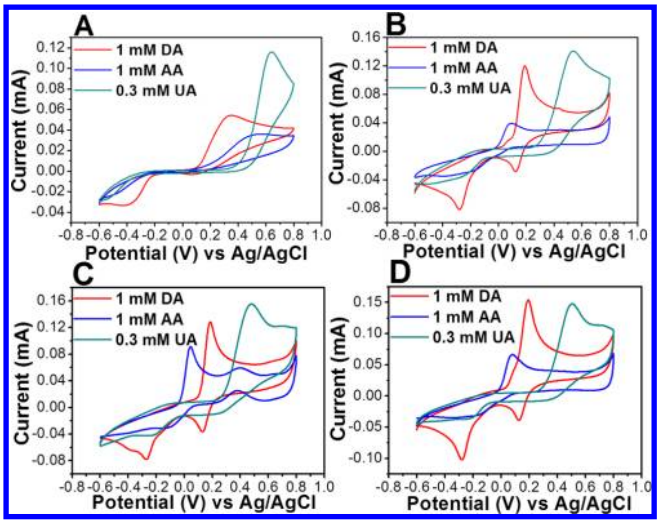

Figure 4. First cyclic voltammograms (scan rate 50 mV/s) of DA (1 mM), AA (1 mM), and UA (0.3 mM) in PBS on nanostructured Au electrodes: (A) film, (B) NC, (C) NS, and (D) NW.

As shown in Figure 4, signals from AA and UA on the film electrode may interfere with that from DA because they oxidize at similar potentials. This would result in overlapping responses. In contrast, the oxidation peaks of AA, UA, and DA separate well on the nanostructured Au electrodes. Nevertheless, determining DA in the presence of AA is still a challenge. This is due to the homogeneous catalytic reaction between AA and DA.[53] The oxidized product of DA, protonated DAQ, can be chemically reduced by AA back to DA. Thus, if this catalytic reaction pathway is hampered, the amount of DA could be detected accurately.[8,12,53] To verify the effect from possible interfering species, citric acid (CA, 1 mM), UA (saturated), and AA (1 μM) are added sequentially into a PBS (0.1 M, pH 7.40) at 0.200 V (Figure 5).[54] For all electrodes, no significant amperometric responses are observed. Further additions of a measured amount of DA display distinguishable step-shaped signals clearly. The reasons why the nanostructured Au electrodes can separate DA and AA oxidations are explained in literature.[55] In addition, the high surface areas of the nanostructures enhance their catalytic activities toward AA. This separates the oxidation peaks effectively.[8,50,56] However, in solutions containing higher amount of AA, the amperometric signals deviate appreciably. The observation suggests that in order to detect DA in real samples directly, further modification of the electrode surface is essential.

CONCLUSION

In this study, high surface area Au nanostructures (NC, NS, and NW) on flexible PET substrates are investigated as potential electrochemical DA sensors. As summarized in Table 3, the preliminary results demonstrate that these unmodified electrodes exhibit higher sensitivities, wider linear ranges, and lower

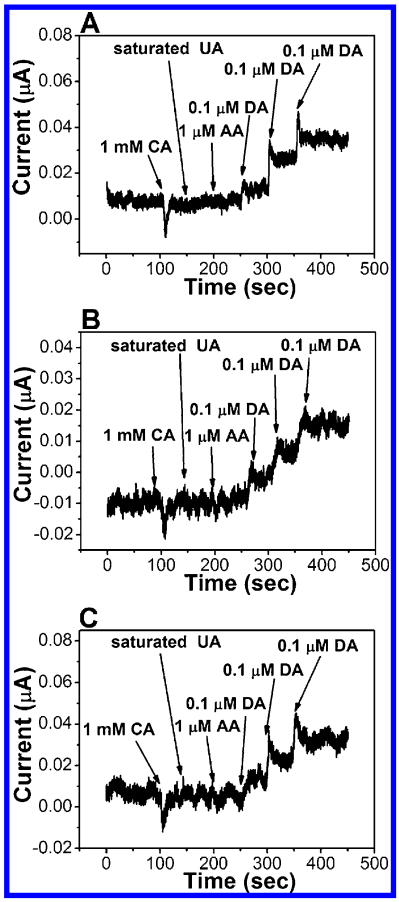

Figure 5. Amperometric responses (0.200 V) on Au electrodes: (A) NC, (B) NS, and (C) NW. Injection sequences (in PBS) are CA (1 mM), UA (saturated), and AA (1 μM), followed by DA (0.1 μM) additions.

Table 3. Summary of Performance of Au Electrodes Towards DA Detection

electrode materials[a]	method	linear range (μM)	detection limit (μM)	ref
NC/PET	amperometry	0.2−500	0.060	this work
NS/PET	amperometry	0.2−600	0.054	this work
NW/PET	amperometry	0.2−600	0.026	this work
NW/glass	amperometry	0.4−250	0.4	57
NPG/GCE	DPV	2−14	0.017	50
NPG/ITO	DPV	1.5−27.5	1.5	46
NPGF/Au	DPV	5−30 nM	1 nM	51

[a]PET: polyethylene terephthalate; NPG: nanoporous gold; GCE: glassy carbon electrode; NPGF: nanoporous gold film; ITO: indium tin oxide.

detection limits than comparable cases reported in literature. In addition, the performance of our simple electrodes matches those of the more complexly structured composite electrodes, as listed in Table S3 in the Supporting Information. Even though the selectivity of the nanostructured Au electrodes needs improvement, we anticipate that they may be used in practical applications after further developments. These include modification of the electrode surfaces to enhance their selectivity, fabrication of the electrodes into arrays, and incorporation the electrodes with capillary electrophoresis apparatus.[58,59] As a result, we anticipate that the flexible electrodes possess great potential for highly sensitive sensor and novel electrochemical device applications.

EXPERIMENTAL SECTION

Chemicals. Hydrogen tetrachloroaurate (III) ($HAuCl_4{\cdot}3H_2O$, 99%), phosphate dibasic dihydrate ($Na_2HPO_4{\cdot}2H_2O$, 99.5%), DA·HCl, UA, AA, and CA (>99%) were purchased from Sigma Aldrich. Cetyltrimethylammonium chloride (CTAC) (890 mM) was supplied by Taiwan Surfactant. Sodium nitrate ($NaNO_3$, 99.9%) was provided by Riedel-de Haën. Sulfuric acid (H_2SO_4, 96.1%) and sodium phosphate ($NaH_2PO_4{\cdot}H_2O$, 99.6%) were bought from J.T. Baker. The as-received chemicals were analytical grade and used without further purification. Deionized (D.I.) water (Milli-Q grade, >18 MΩ) was used throughout. PET transparencies, acquired from Schmidt Film, were used as the flexible growth substrates.

Preparation of Growth Substrate. A thin Ti adhesion layer (thickness: 20 nm) was deposited on a PET transparency by using an e-gun evaporation system (ULVAC EBX-8C). Then, a Au thin film (thickness: 80 nm) was deposited on the Ti layer by the e-gun system. The fabrication steps of the layered structure on the PET substrate are shown in Figure S1 in the Supporting Information. The growth substrate was also used as the film electrode in this study.

Fabrication of Nanostructured Au Electrodes. Au nanostructures were grown electrochemically on the as prepared flexible PET substrates according to literature methods.[34−36] Proper amounts of $HAuCl_4{\cdot}3H_2O$, CTAC, and $NaNO_3$ were mixed in D.I. water to prepare the growth solution. The concentration of each component in the solution was $HAuCl_4{\cdot}3H_2O$ (5 mM), CTAC (10 mM), and $NaNO_3$ (20 mM). After the mixture was sonicated for 5 min, it was placed in a simple two-electrode electrochemical deposition system shown in Figure S3 (Supporting Information). The Au/Ti/PET substrate was used as the cathode while a carbon substrate fabricated from a dried carbon pasted on a PET transparency was employed as the anode. The applied voltage and temperature were summarized in Table S1 (Supporting Information) for each of the experiments. After a designated period of time, nanostructured Au was deposited on the cathode surface. Finally, after the as prepared Au electrode was rinsed with alcohol (Sigma-Aldrich, 97%) and D.I. water, it was dried in a stream of N_2(g). The electrode was stored in a refrigerator (−4 °C) for further investigations.

Instruments. The SEM images and the EDS data were taken from a Hitachi S-4000 (25 keV) and a JEOL JSM-7401F (15 keV). The TEM images and the SAED patterns were captured by a JEOL JEM-3000F (300 kV). The XRD data were obtained from a Bruker AXS D8 Advance.

Electrochemical Experiments. Electrochemical depositions were performed with a DC power supply GW Instek GPS-1830D. CV and amperometric experiments were carried out using an electrochemical potentiostat CH Instruments CHI 6081C. The three-electrode system contained a nanostructured Au electrode (0.5 cm × 0.5 cm) as the working electrode, a Pt wire as the counter electrode, and a Ag/AgCl half-cell (in KCl 3.0 M) as the reference electrode. Before the CV and the amperometric measurements, the nanostructured Au electrodes were cleaned by CV scans in H_2SO_4(aq) (0.5 M). In a typical amperometric experiment, the applied potential was fixed at 0.200 V while DA was successively added of DA into a stirred PBS (0.1 M, pH 7.40) solution.

ASSOCIATED CONTENT

Supporting Information

Tables of growth conditions, voltammetric characteristics, and literature summaries, optical images, SEM and TEM images, ED patterns, substrate fabrication steps, electrochemical deposition apparatus, reduction current responses, cyclic voltammograms, and data of amperometric current responses. This material is available free of charge via the Internet at http://pubs.acs.org.

AUTHOR INFORMATION

Corresponding Author

*E-mail: htchiu@faculty.nctu.edu.tw.

Notes

The authors declare no competing financial interest.

ACKNOWLEDGMENTS

We thank the support from the National Science Council, "Aim for the Top University Plan", of the National Chiao Tung University, and the Ministry of Education of Taiwan, the Republic of China.

REFERENCES

(1) Basu, S.; Dasgupta, P. S. *J. Neuroimmunol.* **2000**, *102*, 113−124.
(2) Hirsch, E.; Graybiel, A. M.; Agid, Y. A. *Nature* **1988**, *334*, 345−348.
(3) Davis, K. L.; Kahn, R. S.; Ko, G.; Davidson, M. *Am. J. Psychiatry* **1991**, *148*, 1474−1486.
(4) LaHoste, G. J.; Swanson, J. M.; Wigal, S. B.; Glabe, C.; Wigal, T.; King, N.; Kennedy, J. L. *Mol. Psychiatry* **1996**, *1*, 121−124.
(5) Long, J. P.; Heintz, S.; Cannon, J. G.; Kim, J. *J. Pharmacol. Exp. Ther.* **1975**, *192*, 336−342.
(6) Sun, C.-L.; Lee, H.-H.; Yang, J.-M.; Wu, C.-C. *Biosens. Bioelectron.* **2011**, *26*, 3450−3455.
(7) Huang, J.; Liu, Y.; Hou, H.; You, T. *Biosens. Bioelectron.* **2008**, *24*, 632−637.
(8) Raj, C. R.; Okajima, T.; Ohsaka, T. *J. Electroanal. Chem.* **2003**, *543*, 127−133.
(9) Kang, T.-F.; Shen, G.-L.; Yu, R.-Q. *Anal. Chim. Acta* **1997**, *354*, 343−349.
(10) Kristensen, E. W.; Kuhr, W. G.; Wightman, R. M. *Anal. Chem.* **1987**, *59*, 1752−1757.
(11) Forzani, E. S.; Rivas, G. A.; Solis, V. M. *J. Electroanal. Chem.* **1995**, *382*, 33−40.
(12) Dalmia, A.; Liu, C. C.; Savinell, R. F. *J. Electroanal. Chem.* **1997**, *430*, 205−214.
(13) Li, J.; Yang, J.; Yang, Z.; Li, Y.; Yu, S.; Xu, Q.; Hu, X. *Anal. Methods* **2012**, *4*, 1725−1728.
(14) Oztekin, Y.; Tok, M.; Bilici, E.; Mikoliunaite, L.; Yazicigil, Z.; Ramanaviciene, A.; Ramanavicius, A. *Electrochim. Acta* **2012**, *76*, 201−207.
(15) Li, Y.; Lin, X. *Sens. Actuators, B* **2006**, *115*, 134−139.
(16) Kalimuthu, P.; John, S. A. *Talanta* **2010**, *80*, 1686−1691.
(17) Ensafi, A. A.; Taei, M.; Khayamian, T.; Arabzadeh, A. *Sens. Actuators, B* **2010**, *147*, 213−221.
(18) Chou, J.; Ilgen, T. J.; Gordon, S.; Ranasinghe, A. D.; McFarland, E. W.; Metiu, H.; Buratto, S. K. *J. Electroanal. Chem.* **2009**, *632*, 97−101.
(19) Hou, S.; Kasner, M. L.; Su, S.; Patel, K.; Cuellari, R. *J. Phys. Chem. C* **2010**, *114*, 14915−14921.
(20) Njagi, J.; Chernov, M. M.; Leiter, J. C.; Andreescu, S. *Anal. Chem.* **2010**, *82*, 989−996.
(21) Min, K.; Yoo, Y. J. *Talanta* **2009**, *80*, 1007−1011.
(22) Shervedani, R. K.; Amini, A. *Bioelectrochemistry* **2012**, *84*, 25−31.
(23) Kim, S.-S.; Nah, Y.-C.; Noh, Y.-Y.; Jo, J.; Kim, D.-Y. *Electrochim. Acta* **2006**, *51*, 3814−3819.
(24) Sun, Y.; Wang, H. H. *Appl. Phys. Lett.* **2007**, *90*, 213103−213107.
(25) Hong-Bo, Z.; Gang, L.; Xiao-Na, S.; Zhuang-Hui, Z.; Qing-Hui, J.; Jian-Long, Z.; Qiu-Shi, R. *J. Microelectromech. Syst.* **2009**, *18*, 88−96.
(26) Li, C.; Han, J.; Ahn, C. H. *Biosens. Bioelectron.* **2007**, *22*, 1988−1993.
(27) Johnson, M. D.; Franklin, R. K.; Gibson, M. D.; Brown, R. B.; Kipke, D. R. *J. Neurosci. Methods* **2008**, *174*, 62−70.
(28) Tijero, M.; Gabriel, G.; Caro, J.; Altuna, A.; Hernandez, R.; Villa, R.; Berganzo, J.; Blanco, F. J.; Salido, R.; Fernandez, L. J. *Biosens. Bioelectron.* **2009**, *24*, 2410−2416.
(29) Choi, B. G.; Park, H.; Park, T. J.; Yang, M. H.; Kim, J. S.; Jang, S.-Y.; Heo, N. S.; Lee, S. Y.; Kong, J.; Hong, W. H. *ACS Nano* **2010**, *4*, 2910−2918.
(30) Chuang, M.-C.; Yang, Y.-L.; Tseng, T.-F.; Chou, T.; Lou, S.-L.; Wang, J. *Talanta* **2010**, *81*, 15−19.
(31) Pradhan, D.; Niroui, F.; Leung, K. T. *ACS Appl. Mater. Interfaces* **2010**, *2*, 2409−2412.
(32) Tsai, T.-C.; Guo, C.-X.; Han, H.-Z.; Li, Y.-T.; Huang, Y.-Z.; Li, C.-M.; Chan, J.-J. J. *Analyst* **2012**, *137*, 2813−2820.
(33) Huang, T.-K.; Chen, Y.-C.; Ko, H.-C.; Huang, H.-W.; Wang, C.-H.; Lin, H.-K.; Chen, F.-R.; Kai, J.-J.; Lee, C.-Y.; Chiu, H.-T. *Langmuir* **2008**, *24*, 5647−5649.
(34) Cheng, T.-M.; Huang, T.-K.; Lin, H.-K.; Tung, S.-P.; Chen, Y.-L.; Lee, C.-Y.; Chiu, H.-T. *ACS Appl. Mater. Interfaces* **2010**, *2*, 2773−2780.
(35) Yang, Y.-C.; Huang, T.-K.; Chen, Y.-L.; Mevellec, J.-Y.; Lefrant, S.; Lee, C.-Y.; Chiu, H.-T. *J. Phys. Chem. C* **2011**, *115*, 1932−1939.
(36) Chen, Y.-L.; Lee, C.-Y.; Chiu, H.-T. *J. Mater. Chem. B* **2012**, accepted.
(37) Wu, H.-L.; Chen, C.-H.; Huang, M. H. *Chem. Mater.* **2008**, *21*, 110−114.
(38) Kumar, S.; Yang, H.; Zou, S. *J. Phys. Chem. C* **2007**, *111*, 12933−12938.
(39) Murphy, C. J.; Jana, N. R. *Adv. Mater.* **2002**, *14*, 80−82.
(40) Trasatti, S.; Petrii, O. A. *J. Electroanal. Chem.* **1992**, *327*, 353−376.
(41) Raina, S.; Kang, W. P.; Davidson, J. L. *Diamond Relat. Mater.* **2009**, *18*, 574−577.
(42) Hawley, M. D.; Tatawawadi, S. V.; Piekarski, S.; Adams, R. N. *J. Am. Chem. Soc.* **1967**, *89*, 447−450.
(43) Ou, C.; Yuan, R.; Chai, Y.; Tang, M.; Chai, R.; He, X. *Anal. Chim. Acta* **2007**, *603*, 205−213.
(44) Shipway, A. N.; Lahav, M.; Willner, I. *Adv. Mater.* **2000**, *12*, 993−998.
(45) Bharathi, S.; Nogami, M.; Ikeda, S. *Langmuir* **2000**, *17*, 1−4.
(46) Ge, P.-Y.; Du, Y.; Xu, J.-J.; Chen, H.-Y. *J. Electroanal. Chem.* **2009**, *633*, 182−186.
(47) Patel, R. B.; Patel, M. R.; Shankar, M. B.; Bhatt, K. K. *Eurasian J. Anal. Chem.* **2009**, *4*, 76−86.
(48) Lane, R. F.; Blaha, C. D. *Langmuir* **1990**, *6*, 56−65.
(49) Lane, R. F.; Hubbard, A. T. *Anal. Chem.* **1976**, *48*, 1287−1293.
(50) Qiu, H.-J.; Zhou, G.-P.; Ji, G.-L.; Zhang, Y.; Huang, X.-R.; Ding, Y. *Colloids Surf., B* **2009**, *69*, 105−108.
(51) Jia, F.; Yu, C.; Ai, Z.; Zhang, L. *Chem. Mater.* **2007**, *19*, 3648−3653.
(52) Gao, Z.; Huang, H. *Chem. Commun.* **1998**, 2107−2108.
(53) Dayton, M. A.; Ewing, A. G.; Wightman, R. M. *Anal. Chem.* **1980**, *52*, 2392−2396.
(54) Concentrations of common species in blood can be found in http://en.wikipedia.org/wiki/Reference_ranges_for_blood_tests.
(55) Bard, A. J.; Faulkner, L. R. *Electrochemical Methods: Fundamentals and Applications*, 2nd ed.; John Wiley & Sons Inc.: New York, 2001.
(56) Zuo, F.; Luo, C.; Zheng, Z.; Ding, X.; Peng, Y. *Electroanalysis* **2008**, *20*, 894−899.
(57) Tyagi, P.; Postetter, D.; Saragnese, D. L.; Randall, C. L.; Mirski, M. A.; Gracias, D. H. *Anal. Chem.* **2009**, *81*, 9979−9984.
(58) Koehne, J. E.; Marsh, M.; Boakye, A.; Douglas, B.; Kim, I. Y.; Chang, S.-Y.; Jang, D.-P.; Bennet, K. E.; Kimble, C.; Andrews, R.; Meyyappan, M.; Lee, K. H. *Analyst* **2011**, *136*, 1802−1805.
(59) Richter, E. M.; da Silva, J. A. F.; Gutz, I. G. R.; do Lago, C. L.; Angnes, L. *Electrophoresis* **2004**, *25*, 2965−2969.